Technical Memorandum 33-702

Effects of Turbulence in the Atmosphere of Venus on Pioneer Venus Radio–Phase II

R. T. Woo and W. Kendall

PREFACE

This report presents the results of one phase of research carried out at the Jet Propulsion Laboratory, California Institute of Technology, for the NASA-Ames Research Center by agreement with the National Aeronautics and Space Administration under Contract NAS7-100.

ACKNOWLEDGMENT

We wish to thank G. Anenberg for his assistance in computing the integrals in Section I and R. Berwin for his programming efforts leading to the results in Section II.

CONTENTS

CONTENTS (Contd)

FIGURES

Abstract

In this report we study two problems related to the effects of turbulence in the atmosphere of Venus on the Pioneer Venus entry probe radio link. In the first, the cross correlation between the log-amplitude and phase fluctuations of the Pioneer Venus communications link is examined. It is seen that for fluctuation frequencies above approximately 1 Hz there is little or no correlation. For frequencies below, the correlation is weak and the square root of the coherence has a peak value close to 0.65. The second problem consists of inferring the turbulence characteristics of the Venus atmosphere from the Mariner 5 phase fluctuations. It is seen that with the data processing techniques developed and currently available, the phase error due to oscillator drift, assumed trajectory delay and spline-curve fit exceed the turbulence induced fluctuations. It is, therefore, not possible to infer the turbulence characteristics from the Mariner 5 phase fluctuations.

I. Cross Correlation Between the Amplitude and Phase Fluctuations of the Pioneer Venus Entry Probe Communications Link

1.1 Introduction

Before the effects of a turbulent medium on a communications link can be realistically assessed, the statistics and characteristics of both amplitude and phase fluctuations induced in a radio signal propagating through the turbulent medium must be known. In our previous study (Ref. 1), we discussed in detail the distributions, means, variances and power spectra of the amplitude and phase fluctuations in the Pioneer Venus entry probe radio link. Also of interest is the degree to which the amplitude and phase fluctuations are correlated (Ref. 2); in other words, we wish to obtain information on the cross spectrum and coherence between the amplitude and phase fluctuations. Although the formulation for analyzing these correlation characteristics has recently been given (Ref. 3), no detailed results have been computed or published. The purpose of this report is to present calculations carried out and applied to the Pioneer Venus configuration.

1.2 Formulation of Problem

An electric field propagating in free space can be written as

$$u_o(r) = A_o(r) \, e^{i\phi_o(r)} \tag{1}$$

where A_o is the amplitude and ϕ_o the phase. If the medium is turbulent, the electric field becomes

$$u(r,t) \quad = \quad A(r,t) \; e^{i\phi(r,t)} \tag{2}$$

Using Rytov's method to solve Maxwell's equations, it can be shown (Ref. 4) that

$$u(r,t) \quad = \quad u_o(r) \; e^{\psi(r,t)} \tag{3}$$

where $\psi = \chi + iS$, and $\chi = \ell n \dfrac{A}{A_o}$ is the log-amplitude fluctuations while $S = \phi - \phi_o$ is the phase fluctuation. Ishimaru (Ref. 3) has shown that if $B_{\chi S}$ is the cross correlation between the log-amplitude and phase fluctuations, then the temporal frequency spectrum $W_{\chi S}$ of the cross correlation between the log-amplitude and phase fluctuations defined by

$$W_{\chi S}(f) \quad = \quad 2 \int_{-\infty}^{\infty} B_{\chi S} \; e^{-i\omega\tau} \; d\tau \tag{4}$$

where f is the fluctuation frequency and $\omega = 2\pi f$, is given by

$$W_{\chi S}(f) \quad = \quad 8\pi k^2 L' \int_{\omega/v}^{\infty} f_{\chi S}(\kappa) \; \Phi_n(\kappa) \; \frac{\kappa d\kappa}{[(\kappa v)^2 - \omega^2]^{\frac{1}{2}}} \tag{5}$$

where κ is the spatial wave number, $\Phi_n(\kappa)$ is the spectrum for the index of refraction fluctuations, v is the wind velocity transverse to the line-of-sight path, k is the free space wave number and L' is the propagation distance. For spherical wave propagation

$$f_{\chi S}(\kappa) \quad = \quad \frac{1}{L'} \int_{0}^{L'} d\eta \; \text{Im}[-hh* - h^2] \tag{6}$$

where

$$h = \exp\left[-i \frac{\eta}{L'} (L' - \eta) \frac{\kappa^2}{2\kappa}\right]$$

* denotes complex conjugate, η is the coordinate along the line-of-sight path originating at the transmitter and Im[ ] means imaginary part of [ ].

Another quantity we wish to calculate is the coherence $coh_{\chi S}$ of log-amplitude and phase fluctuations (Ref. 5).

$$coh_{\chi S} = \rho^2(f) = \frac{\left[W_{\chi S}(f)\right]^2}{W_\chi(f) \; W_S(f)} \tag{7}$$

where $W_\chi(f)$ is the frequency spectrum for the log-amplitude fluctuations and $W_S(f)$ is the frequency spectrum for the phase fluctuations. In many analyses the square root of the coherence $\rho(f)$ is used since it is more analogous to the familiar coefficient of correlation (Ref. 6). When $\rho(f) = 1$ the log-amplitude and phase fluctuations are completely coherent at f, while if $\rho(f) = 0$, they are independent at f.

1.3 Application to Pioneer Venus Entry Mission

The Pioneer Venus configuration is depicted in Figure 1. As discussed in our previous report (Ref. 1), we will assume that turbulence in the Venusian atmosphere is homogeneous for altitudes lower than 55 km and non-existent for higher altitudes. From our study based on Mariner 5 (Ref. 7), we have found that the intensity of turbulence actually varies with altitude. The effect of this variation on the gross features of the frequency spectra should be small, so that the results obtained in this report are representative.

Another point worth mentioning is that for the Pioneer Venus entry mission, the Fresnel-zone size $\sqrt{\lambda L}$ (λ is the wavelength and L is defined in Figure 1) is smaller than the outer scale size of turbulence L_o (Ref. 1). Thus, the effects of finite extent and inhomogeneity of turbulence in the direction transverse to the line-of-sight path that need be considered for the cross spectra in a fly-by mission (Ref. 8), can be neglected in the case of Pioneer Venus. As in our previous study (Ref. 1), we will assume that $\Phi_n(\kappa)$ is represented by Kolmogorov's spectrum of the form proposed by von Kármán, i.e.,

$$\Phi_n(\kappa) \quad = \quad 0.033 \ c_n^2 \left(\kappa^2 + \frac{1}{L_o^2}\right)^{-11/6} \tag{8}$$

where c_n, the structure constant for the refractive index fluctuations, characterizes the intensity of turbulence and L_o is the outer scale size of turbulence.

Let us now apply (5) and (6) to the Pioneer Venus configuration shown in Figure 1. We note that $L'' = L' + L$ and since $L'' \gg L$, $\eta(L-\eta)/L$ in (6) becomes simply η. We then integrate (6) and obtain

$$f_{\chi S}(\kappa) \quad = \quad \frac{2k}{\kappa^2 L} \ \sin^2 \left(\frac{\kappa^2 L}{2k}\right) \tag{9}$$

Also, (5) can be rewritten

$$W_{\chi S}(f) \quad = \quad \frac{8\pi^2 k^2 L}{v} \int_0^\infty f_{\chi S}\left(\sqrt{\kappa'^2 + \frac{\omega^2}{v^2}}\right) \ \Phi_n\left(\sqrt{\kappa'^2 + \frac{\omega^2}{v^2}}\right) \ d\kappa' \tag{10}$$

In the next section we will evaluate (10) and subsequently (7).

1.4 Results and Discussion

Using the second solution of the confluent differential equation (Ref. 8), (10) along with (9) can be expressed in the following closed form:

$$W_\chi (f) = 0.033 \, c_n^2 \, \frac{4\pi^2 k^3}{v} \left(\frac{\omega}{v}\right)^{-14/3} \Gamma\left(\frac{1}{2}\right)$$

$$\cdot \left\{ \frac{\Gamma\left(\frac{7}{3}\right)}{\Gamma\left(\frac{17}{6}\right)} - \text{Re}\left[e^{i\alpha^2} \, \psi\left(\frac{1}{2}, \; -\frac{4}{3}; \; -i\alpha^2\right)\right] \right\} \qquad (11)$$

where $\alpha = \dfrac{f}{f_\perp}$, $f_\perp = \dfrac{v}{2\pi}\sqrt{\dfrac{k}{L}}$, Re[ ] means real part of [ ], Γ is the Gamma function and $\psi(a, c; z)$ is the confluent hypergeometric function which is independent of the Kummer function. Let us examine the asymptotic forms of (10) when $f \to 0$ and $f \to \infty$.

For the case $f \to 0$, we write $\psi(a, c; z)$ in terms of the Kummer function $\phi(a, c; z)$ (Ref. 9)

$$\psi(a, c; z) = \frac{\Gamma(1-c)}{\Gamma(a-c+1)} \, \phi(a, c; z)$$

$$+ \frac{\Gamma(c-1)}{\Gamma(a)} \, z^{1-c} \, \phi(a-c+1, \, 2-c; \, z) \qquad (12)$$

and then use the small argument approximation for $\phi(a, c; z)$ (Ref. 9)

$$\phi(a, c; z) = 1 + \frac{a}{c} z \qquad (13)$$

We finally obtain

$$W_{\chi S}(f) = 0.033 \, c_n^2 \, \frac{4\pi^2}{v} \, L^{7/3} \, k^{2/3} \, \Gamma\left(\frac{1}{2}\right) \frac{\Gamma\left(\frac{7}{3}\right)}{\Gamma\left(\frac{17}{6}\right)} \frac{55}{32} \, \alpha^{-2/3} \qquad (14)$$
$$f \to 0$$

For convenience of plotting we will normalize (14) to $W_\chi(0)$ as given in Ref. 3, i.e.,

$$W_\chi(0) = 0.033 \, c_n^2 \, \frac{4\pi^2}{v} \, L^{7/3} \, k^{2/3} \, \frac{\pi}{2\left(\frac{10}{3}\right)\sin\frac{\pi}{3}} \qquad (15)$$

We then have

$$\frac{W_{\chi S}(0)}{W_\chi(0)} = \frac{55}{16} \frac{\Gamma\left(\frac{7}{3}\right)}{\Gamma\left(\frac{17}{6}\right)} \frac{\Gamma\left(\frac{10}{3}\right)\sin\frac{\pi}{3}}{\sqrt{\pi}} \, \alpha^{-2/3} = 3.23 \, \alpha^{-2/3} \qquad (16)$$

For the case $f \to \infty$, we employ the large argument approximation for $\psi(a, c; z)$ in (11) (Ref. 9):

$$\psi(a, c; z) = z^{-a} \qquad (17)$$

and again normalizing to $W_\chi(0)$ we obtain

$$\frac{W_{\chi S}(\infty)}{W_\chi(0)} = \frac{2\sin\frac{\pi}{3} \, \Gamma\left(\frac{1}{2}\right) \, \Gamma\left(\frac{10}{3}\right) \, \Gamma\left(\frac{7}{3}\right)}{\pi \, \Gamma\left(\frac{17}{6}\right)} \, \alpha^{-14/3} = 1.88 \, \alpha^{-14/3} \qquad (18)$$

So far we only have the asymptotic solutions $W_{\chi S}$ normalized to $W_\chi(0)$. To calculate the intermediate values we used the Univac 1108 digital computer to integrate (5). The method employed was the trapezoidal rule together with Romberg's extrapolation method (Ref. 10). Shown in Figure 2 are the results of $W_{\chi S}(f)$ normalized to $W_\chi(0)$ and plotted as a function of α for various values of $\beta = \dfrac{1}{L_0} \sqrt{\dfrac{L}{k}}$. These values of β correspond to $L_0 = 50$, 100 and ∞ m for $L = 55$ km at $f = 2300$ MHz. As can be seen the fluctuations in all cases occur primarily at frequencies less than $2f_\perp$. For $L = 55$ km, and assuming $v = 50$ m/sec, $2f_\perp = 0.47$ Hz.

Calculations for the square root of coherence ρ have also been made and the results are plotted in Figure 3. The coherence results show that there is no correlation between the log-amplitude and phase fluctuations for $f \gtrsim 2f_\perp$. When $f \lesssim 2 f_\perp$ there is some correlation with the peak of ~ 0.65 occurring at $f \sim f_\perp$.

The results discussed so far assume that the sub-earth direction corresponds to the zenith of Venus (Figure 1). If the sub-earth direction makes an angle θ with the zenith of Venus, then L in (10) must be replaced by L sec θ, while v by v cos θ.

1.5 Conclusions

We have studied the cross correlation between the log-amplitude and phase fluctuations of the Pioneer Venus entry probe radio link. It is seen that for fluctuation frequencies above 1 Hz or so there is no correlation. For frequencies below, the log-amplitude and phase fluctuations are weakly correlated with the peak in ρ occurring at $f \sim f_\perp$ and having a value close to 0.65.

II. The Study of Small-Scale Turbulence in the Atmosphere of Venus Using the Mariner 5 Phase Fluctuations

2.1 Introduction

As discussed in our previous report (Ref. 1), prediction of the effects of turbulence in the Venus atmosphere on the radio link of Pioneer Venus entry probes relies heavily on radio measurements of the turbulence made by previous space probes. We have studied the amplitude fluctuations of the S-band signal received from Mariner 5 when it flew behind Venus. The results yielded the most comprehensive measurements of the small-scale turbulence characteristics of the Venus atmosphere for altitudes higher than 35 km (Ref. 7). In this report, we wish to examine the possibility of deriving similar information based on the Mariner 5 phase fluctuations. In Sections 2.2 to 2.5 we discuss the processing steps for extracting the turbulence-induced phase fluctuations from the Mariner 5 radio data, while the results are discussed in Section 2.6.

2.2 Extraction of Phase Data from the Received Signal

The signal transmitted from the Mariner 5 spacecraft through the atmosphere of Venus is received on earth at a later time due to delays which can be attributed to (1) the propagation time required for the signal to propagate from the spacecraft to the earth, (2) the delay caused by the "average", or non-turbulent, Venusian atmosphere, and (3) deviations from this average caused by turbulence and other atmospheric non-homogeneities. It is this last component which is to be analyzed.

The delay which is to be measured is manifested in the received signal as a phase modulation of the received carrier. The receiving and processing steps to which the signal is subjected are designed to extract this phase modulation, and then to identify which of its components are due to turbulence. Then these components are extracted and spectrum analyzed.

2.3 Phase-Locked-Loop Processing

The signal $v(t)$ from the receiving and pre-processing operations described in Appendix A of Reference 1 is

$$v(t) \quad = \quad A(t) \ \sqrt{2} \ \sin\left\{2\pi[(\Delta/2)t - f_{sc}d_n(t)] + k_1\right\} \ + \ n(t) \qquad (19)$$

where

$A(t)$ = rms received signal amplitude (time varying),

Δ = final signal bandwidth processed (Hz),

f_{sc} = carrier frequency transmitted from spacecraft,

$d_n(t)$ = delay caused by non-homogeneities in the Venusian

atmosphere and other uncertainties (time varying),

k_1 = arbitrary constant phase offset (radians),

$n(t)$ = receiver noise added to the received signal.

In order to quantitatively determine the effects of planetary turbulence, it is

necessary to extract (or estimate) the amplitude $A(t)$ [as described in Ref. 1]

and the phase $f_{sc}d_n(t)$ from the signal $v(t)$. This is accomplished by computer

processing which extracts these parameters with a digital phase-locked-loop

(PLL).

It is important to note that the delay component $d_n(t)$ consists not only

of the delay caused by non-homogeneities in the Venusian atmosphere, but also

other uncertainties. These other uncertainties include (1) error in the assumed

transmitted frequency f_{sc} due to oscillator drift, (2) error in the assumed

trajectory delay component, and (3) error in the assumed average atmosphere

delay component (the so-called "spline-curve fit error"). These errors must

be recognized and removed in subsequent processing, and the only basis presently

available for doing this is the assumption that these errors are more slowly

varying functions of time than is the turbulence component, so that they can be

filtered out, i.e., separation will be done in the spectral domain.

2.3.1 Phase Extraction

Here we will not give a complete description of the workings of the

phase-locked-loop, since several good references on this subject are readily

available. Instead, we will simply note that the PLL is a non-linear phase-

tracking device which can normally (when it is tracking) be well approximated

as a device whose input is of the form

$$x(t) = A\sqrt{2} \sin\left\{2\pi f_{vco} t + \theta_1(t)\right\} + n(t) \tag{20}$$

where f_{vco} is the quiescent frequency of the PLL's VCO, and which extracts the phase $\theta_1(t)$ from the signal. In the process of doing this, the PLL passes the phase θ_1 and the noise $n(t)$ (scaled by division by the amplitude A) through a lowpass filter to produce θ_2, a noisy estimate of the phase θ_1. In other words, the output phase estimate $\theta_2(t)$ is that which would be obtained by passing the input phase deviation $\theta_1(t)$ through a lowpass filter, plus an error which can be thought of as coming from passing white noise through the same lowpass filter.

When using the PLL to estimate the signal delay component due to atmospheric non-homogeneities, the VCO quiescent frequency is set to the center of the band at $\Delta/2$ so that

$$\theta_1(t) = -2\pi f_{sc}d_n + k_1 \ . \tag{21}$$

The phase estimate $\theta_2(t)$ is then simply noise plus a term proportional to the desired delay component d_n lowpass filtered.

The transfer function of the equivalent lowpass filter of the linearized second-order PLL is (Reference 11, Eq. 5-19)

$$L(s) = \frac{1 + \left(\dfrac{R+1}{4B_L}\right)s}{1 + \left(\dfrac{R+1}{4B_L}\right)s + \left(\dfrac{R+1}{4B_L\sqrt{R}}\right)^2 s^2} \tag{22}$$

$$= \frac{1 + (2\zeta/W_n)s}{1 + (2\zeta/W_n)s + s^2/W_n^2}$$

where

B_L = one-sided loop noise bandwidth (Hz),

R = Tausworthe's damping parameter,

W_n = loop natural radian frequency,

ζ = loop damping factor.

The magnitude and the squared magnitude of the filter transfer function $L(j2\pi f)$ are shown in Figures 4 and 5, respectively.

2.3.2 Phase Errors

The phase estimate $\theta_2(t)$ produced by the PLL will differ from the desired phase $\theta_1 = 2\pi f_{sc}d_n + k_1$, due to two factors, viz., (1) higher-frequency variations in $\theta_1(t)$ will be filtered out by the lowpass filter $L(s)$ (unless the loop bandwidth B_L is made sufficiently large), and (2) the low-frequency components of the noise $n(t)/A$, which in this case has an essentially flat spectrum, will pass through the filter $L(s)$. Thus, it is clear that for the best possible phase-estimate accuracy, the loop bandwidth used should be as small as possible, consistent with the requirement that it pass all significant variations in the input phase θ_1.

If we let

$$\phi = \text{Phase error (rad)}$$

$$= \theta_1(t) - \theta_2(t) \tag{23}$$

and

$$S_\phi(f) = \text{one-sided spectral density of } \phi \text{ due to noise,} \tag{24}$$

then for spectrally flat noise, which is typical of the receiver noise present at the input to the PLL, with one-sided power spectral density N_0 watts/Hz, we get

$$S_\phi(f) \quad = \quad \frac{N_0}{A^2} \quad |L(j2\pi f)|^2 \tag{25}$$

where N_0/A^2 is the spectral density of the noise at the input to the equivalent lowpass filter $L(s)$, and A^2 is the power in the signal into the PLL (see Ref. 12, Sec. 2.8). Thus, the spectral density of the noise-induced phase error will have the shape shown in Figure 5, and a level which depends on the signal-to-noise ratio (SNR) N_0/A^2.

The mean squared value σ_ϕ^2 of the phase error is just

$$\sigma_\phi^2 \quad = \quad \int_0^\infty S_\phi(f) \, df$$

$$= \quad \frac{N_0}{A^2} \int_0^\infty |L(j2\pi f)|^2 \, df \tag{26}$$

$$= \quad \frac{N_0 B_L}{A^2} \quad .$$

In order for the linearized model of the PLL which we have been assuming to be valid, this mean squared phase error must be less than about $0.1(\text{rad})^2$. Thus,

for the PLL processing described here the loop bandwidth B_L was chosen small enough to satisfy

$$\sigma_\phi^2 \;=\; \frac{N_0 B_L}{A^2} \;\leq\; 0.1 \tag{27}$$

$$B_L \;\leq\; \frac{A^2}{10\,N_0} \;=\; \frac{\text{SNR in 1-Hz Bandwidth}}{10} \;. \tag{28}$$

2.4 Spectrum Analysis of the Phase Estimates

Once the phase as a function of time has been estimated by PLL tracking, it is desired to separate this estimate into three components: (1) the fluctuations due to the Venusian atmospheric turbulence, (2) the (slowly varying) errors due to spacecraft oscillator drift, trajectory errors, and errors in the assumed average atmosphere, and (3) the variations due to noise at the receiver input. It was expected that the separation could be made in the spectral domain by the following two steps. First, the phase estimates are "detrended" by passing them through a high-pass digital filter which removes all dc and slowly-varying components from them. Then, the high-pass-filtered signal is spectrum analyzed using an FFT algorithm, and theoretical results are used to identify the noise components.

2.4.1 High-Pass Filtering

Since spectral analysis is a special case of bandpass filtering, it is not always necessary to precede the spectral analysis step by high-pass filtering or "detrending". However, when this is not done and a large dc

or "trend" component is present, the sidelobe response of the bandpass
filters of the spectral analysis will respond to the very large dc component,
and the high-frequency portion of the spectrum will be distorted. For the
phase data spectrum analyzed here, a Butterworth highpass filter of order 4
to 8 was used when the high-frequency portion of the spectrum was being
studied, and no filter was used when the low-frequency portion of the
spectrum was being studied. This was so that when trying to separate the
residual delay errors from the low-frequency turbulence components in the
delay d_n, there would not be any filter artifacts near its cutoff frequency
to degrade the spectra.

2.4.2 Spectrum Analysis

The samples of phase, with or without highpass filtering, were processed
through a fast Fourier transform (FFT) routine to estimate the spectrum of the
signal's phase. This was a conventional FFT routine augmented by two special
features: a Hamming window and zero fill. The purpose of the Hamming window
is to reduce the spurious "sidelobe" response of strong spectral components
(with a corresponding loss in frequency resolution), and the purpose of using
zero fill is simply to evaluate the Fourier transform of the phase estimates
at closer-spaced frequencies than would otherwise be obtained.

2.4.3 Spectrum Normalization

For direct comparison with the theoretical results it is necessary to
maintain the correct spectral level at the output of the spectrum-analysis
processing steps. This means that the effect of the Hamming window must be

accounted for, as well as that care must be used in determining the appropriate normalization at the other steps.

The Hamming window is accounted for by computing the mean-squared value of the phase data both before and after the Hamming window is applied. Then the spectral levels produced by the FFT routine are increased by the ratio of these mean-squared values. This assures that the area under the spectral curve equals the energy in the data, as is required by Parseval's theorem.

2.4.4 Frequency Averaging

The final step in producing the experimental spectra is averaging over frequency. This step is required due to the fact that we are estimating the power spectrum of a random process (the turbulence-induced phase fluctuations) from one sample function of that random process, and estimates obtained this way are very noisy. For example, the standard deviations of such estimates are approximately equal to the mean spectral level. By averaging several adjacent frequency points together, the variances of the estimates are reduced, at the expense of reduced frequency resolution.

The averaging done here is a "running-point" average, i.e., the spectrum at every frequency point is replaced by

$$\hat{G}_{AV}(f) \quad = \quad \frac{1}{m} \sum_{\ell = -(m-1)/2}^{(m-1)/2} \hat{G}(f + \ell\Delta f) \tag{29}$$

where

$\quad\quad m \quad = \quad$ number of points (assumed odd) in running-point average,

$\quad\quad \Delta f \quad = \quad$ frequency spacing from FFT,

$\quad\quad \hat{G}(f) \quad = \quad$ spectrum from FFT at frequency f.

2.5 Interpretation of Results

The last step in the processing consists of using the theoretical
results of this report to separate the turbulence-induced fluctuations from
the noise-induced fluctuations. The noise is recognized [see Equation (25)]
by having the spectral shape shown in Figure 5 and a level given by N_0/A^2.
The part of the experimental spectrum which deviates from this noise part is
then interpreted in terms of turbulence-induced phenomena.

2.6 Results and Discussion

Shown in Figure 6 is the time history of the Mariner 5 signal level during
entrance occultation. The altitudes corresponding to the lowest penetration of
the propagation path are indicated at the top of the figure. As discussed in
Ref. 7, turbulence was found in regions A and C, which correspond to the vicin-
ities of 60 and 45 km, respectively. Region E is of interest also because this
pre-occultation period indicates the "system" noise. Shown in Figure 7 are the
frequency spectra of the log-amplitude fluctuations which were obtained in our
previous study. It is clear that the spectral density levels for regions A and
C are substantially above the spectral density levels of region E and the noise
levels corresponding to regions A and C as well. The frequency spectra obtained
for the phase fluctuations in regions A, C and E are depicted in Figure 8. The
frequency response of the eighth order Butterworth high-pass filter is shown in
Figure 9. The cut-off frequency is 0.1 Hz. As discussed in Section 2.5, the
corresponding noise levels are given by N_0/A^2. These are not shown in Figure 8
because they are lower than the range of spectral density levels plotted. The
theoretical plot is the theoretical frequency spectrum for phase fluctuations

for region A. This has been calculated using the analytical results given in Ref. 13 and the turbulence characteristics derived from the log–amplitude fluctuations (Ref. 7). Contrary to the log–amplitude fluctuations, the frequency spectra for the phase fluctuations for regions A, C and E show no substantial differences. Moreover, the spectral density levels are significantly higher than the theoretically predicted ones. These results indicate that the errors due to oscillator drift, assumed trajectory delay component and spline–curve fit exceed the turbulence induced fluctuations and have not been completely removed by our presently developed processing techniques. Looking at it from a total power point of view, the standard deviation of phase fluctuations due to the errors mentioned above exceeds the standard deviation of phase fluctuations due to turbulence which is estimated to be approximately 6 degrees.

It should be mentioned that a study of Venus atmospheric turbulence based on the Mariner 10 phase fluctuations is currently being carried out. Because of the availability of a coherent S/X link on Mariner 10, the uncertainties present in the Mariner 5 data will hopefully be removed by looking at the phase differences.

2.7 Conclusions

We have studied the Mariner 5 phase fluctuations with the objective of inferring the turbulence characteristics of the Venus atmosphere. It is seen that with the data processing techniques developed and currently available, the phase error due to oscillator drift, assumed trajectory delay and spline–curve fit exceed the turbulence induced fluctuations in

the phase.   It is therefore not possible to infer the turbulence characteristics

from the Mariner 5 phase fluctuations.   Our study of Mariner 10 should, however,

shed more light on this problem, since these errors can be eliminated by looking

at the S/X phase difference.

References

1. R. Woo, W. Kendall, A. Ishimaru, R. Berwin, "Effects of Turbulence in the Atmosphere of Pioneer Venus Radio -- Phase I", Jet Propulsion Laboratory Technical Memorandum 33-644, June 30, 1973.

2. W. C. Lindsey and W. J. Weber, "Phase Lock Loop Performance in the Presence of Fading Communication Channels", to be presented at the IEEE International Conference of Communications, June 1974 in Minneapolis, Minn.

3. A. Ishimaru, "Temporal Frequency Spectra of Multifrequency Waves in Turbulent Atmosphere", IEEE Trans. on Antennas and Propagation, Vol. AP-20, No. 1, January 1972, pp. 10-19.

4. V. I. Tatarski, The Effects of the Turbulent Atmosphere on Wave Propagation. Nauka, Moscow, 1967. Translated and available from the U.S. Dept. of Commerce, Springfield, Virginia.

5. J. S. Bendat and A. G. Piersol, Random Data: Analysis and Measurement Procedures. Wiley-Interscience, New York, 1971.

6. H. B. Janes, M. C. Thompson, D. Smith and A. W. Kirkpatrick, "Comparison of Simultaneous Line-of-sight Signals at 9.6 and 34.5 GHz", IEEE Trans. on Antennas and Propagation, Vol. AP-18, No. 4, July 1970, pp. 447-451.

7. R. Woo, A. Ishimaru and W. Kendall, "Observations of Small-Scale Turbulence in the Atmosphere of Venus by Mariner 5", to be published in J. of the Atmospheric Sciences, September 1974.

8. R. Woo and A. Ishimaru, "Frequency Spectra of Multifrequency Waves in Localized Smoothly Varying Turbulence", to be presented at the 1974 USNC/URSI Meeting, June 11-13, 1974 in Atlanta, Georgia.

9. E. Jahnke, F. Emde and F. Losch, Tables of Higher Functions. McGraw-Hill, New York, 1960, pp. 276-285.

10. S. Filippi, "Das Verfahren von Romberg-Stiefel-Bauer als Spezialfall des allgemeiner Prinzips von Richardson", Mathematik-Technik-Wirtschaft, Vol. 11, No. 2, 1964, pp. 49-54.

11. R. C. Tausworthe, "Theory and Practical Design of Phase-Locked Receivers", Vol. I, Jet Propulsion Laboratory, Pasadena, California, Technical Report No. 32-819, February 15, 1966.

12. A. J. Viterbi, Principles of Coherent Communication, McGraw-Hill, New York, 1966.

13. R. Woo and A. Ishimaru, "Effects of Turbulence in a Planetary Atmosphere on Radio Occultation", to be published in IEEE Trans. on Antennas and Propagation, July 1974.
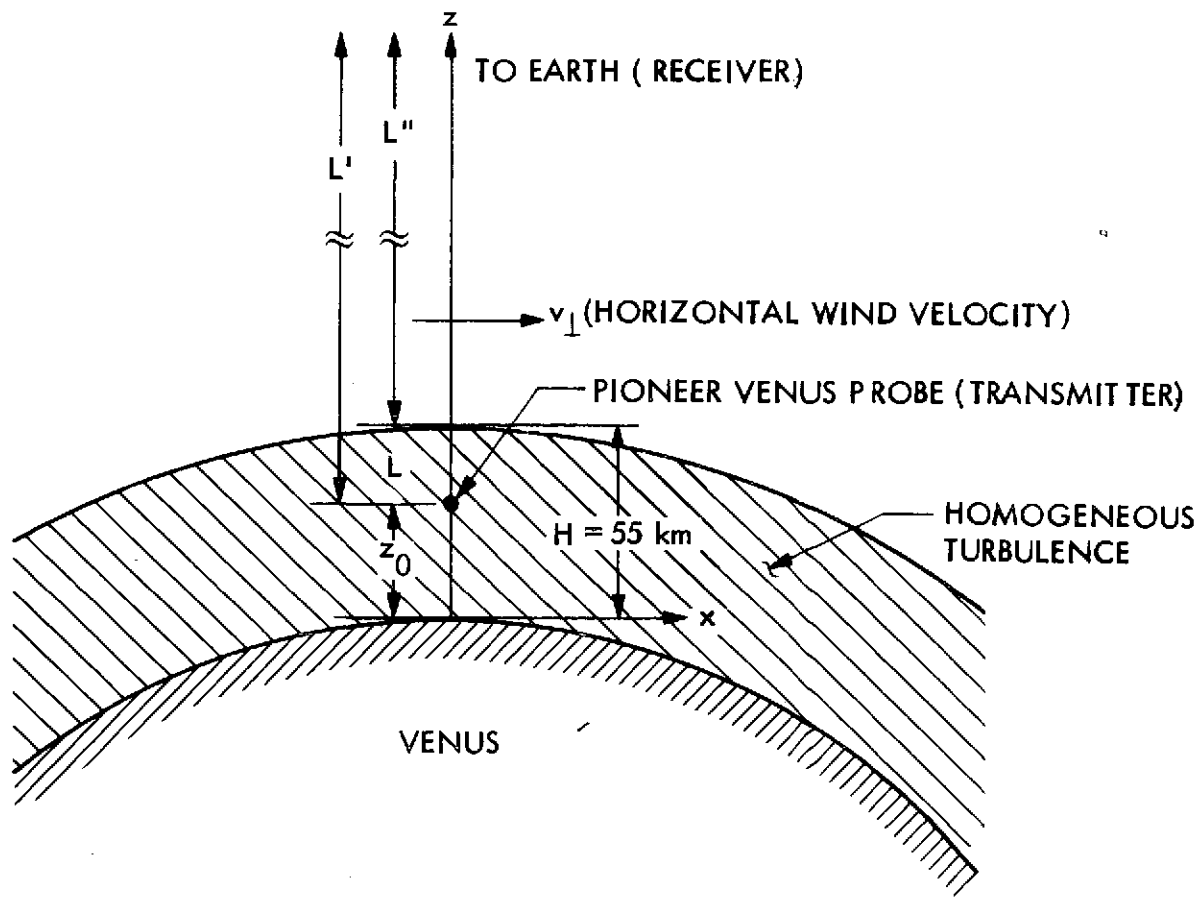
Fig. 1. Pioneer venus entry configuration
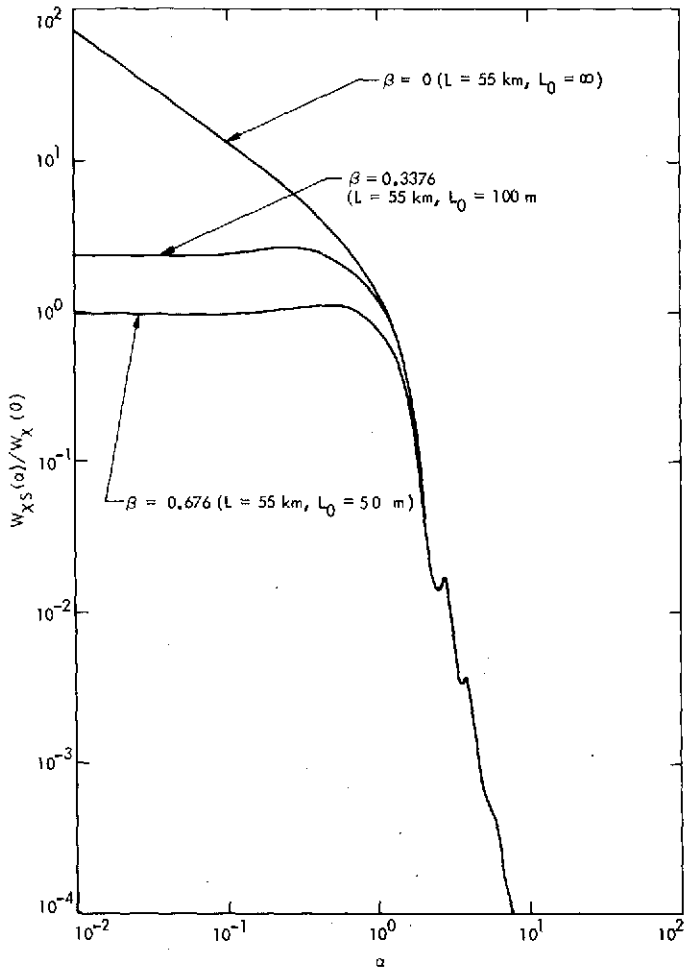
Fig. 2. Normalized cross power spectra of log-amplitude and phase fluctuations
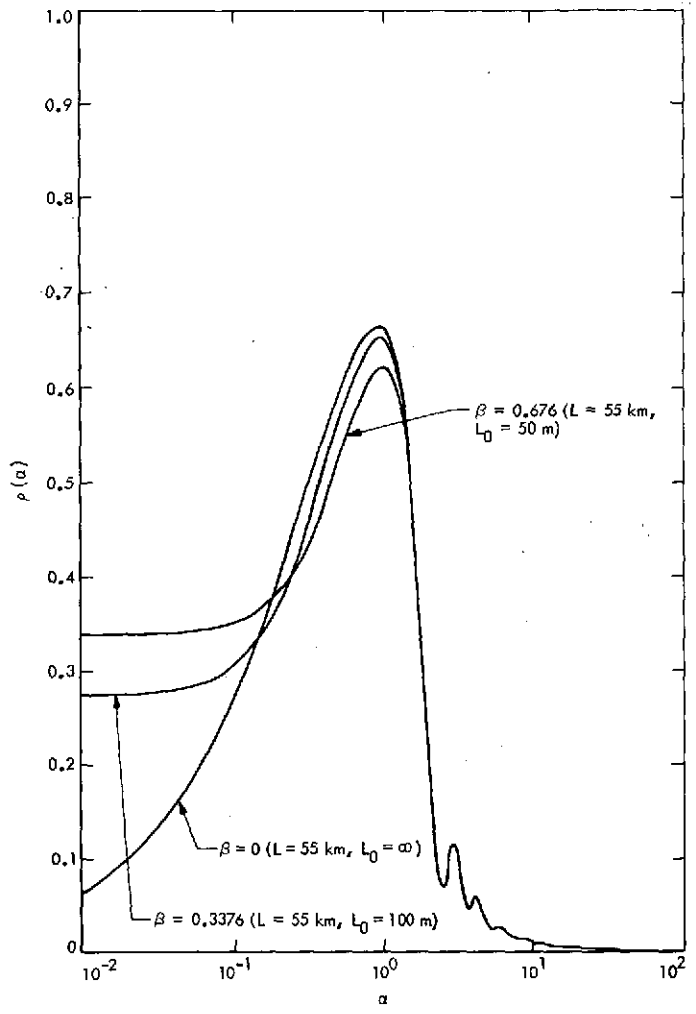
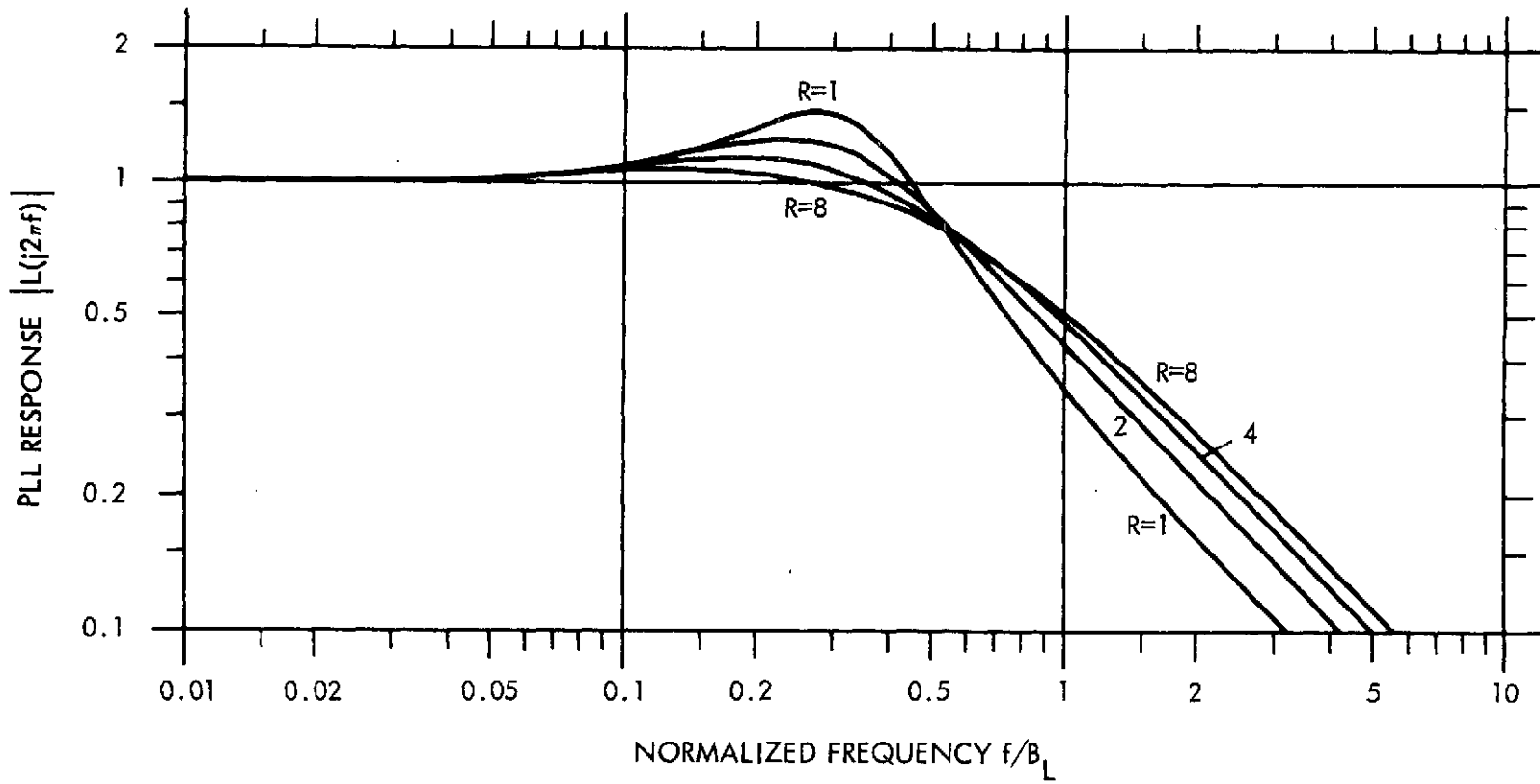Fig. 3. Square root of coherence of log-amplitude and phase fluctuations

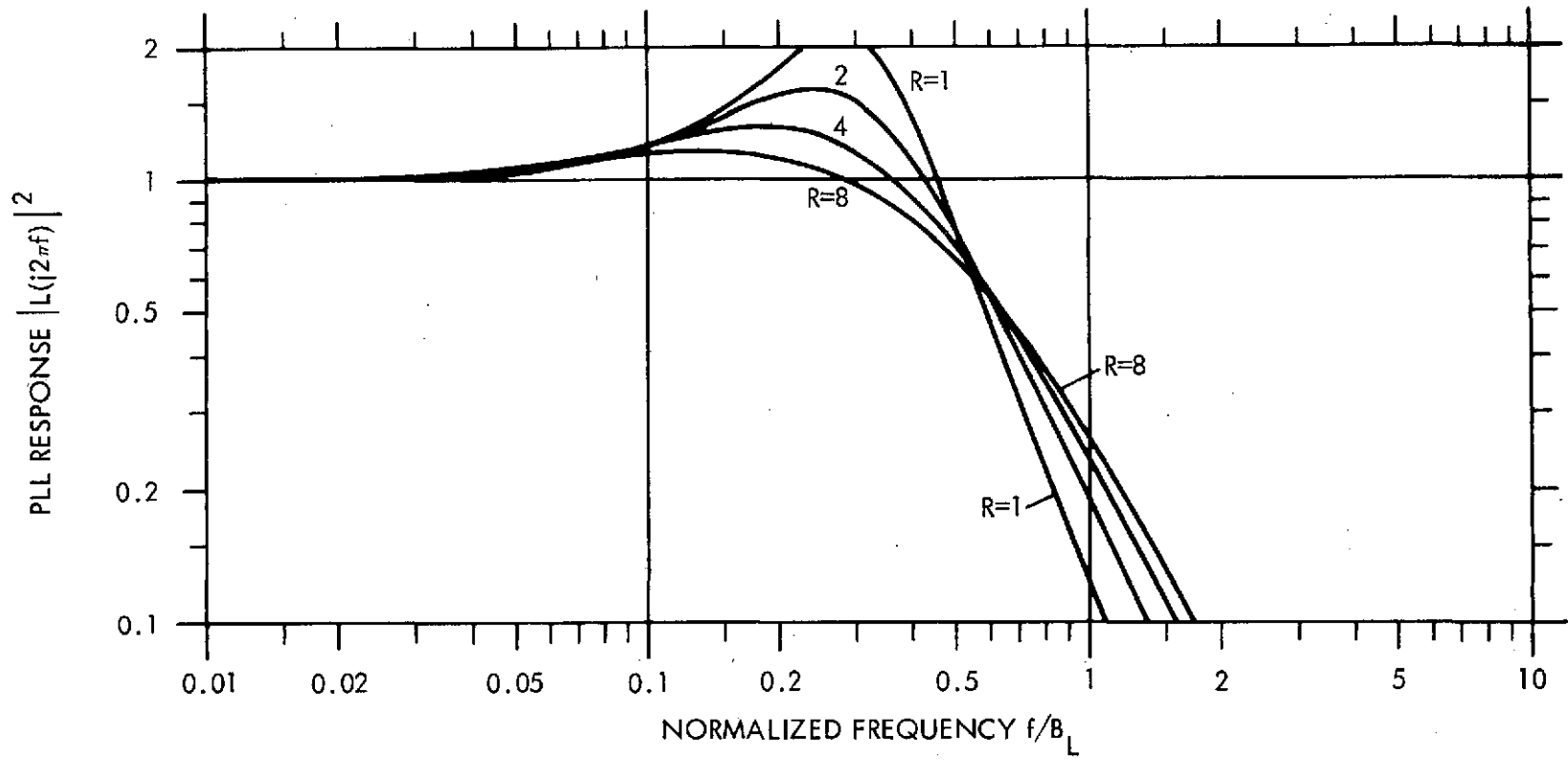Fig. 4. Response of PLL to phase modulation at frequency f

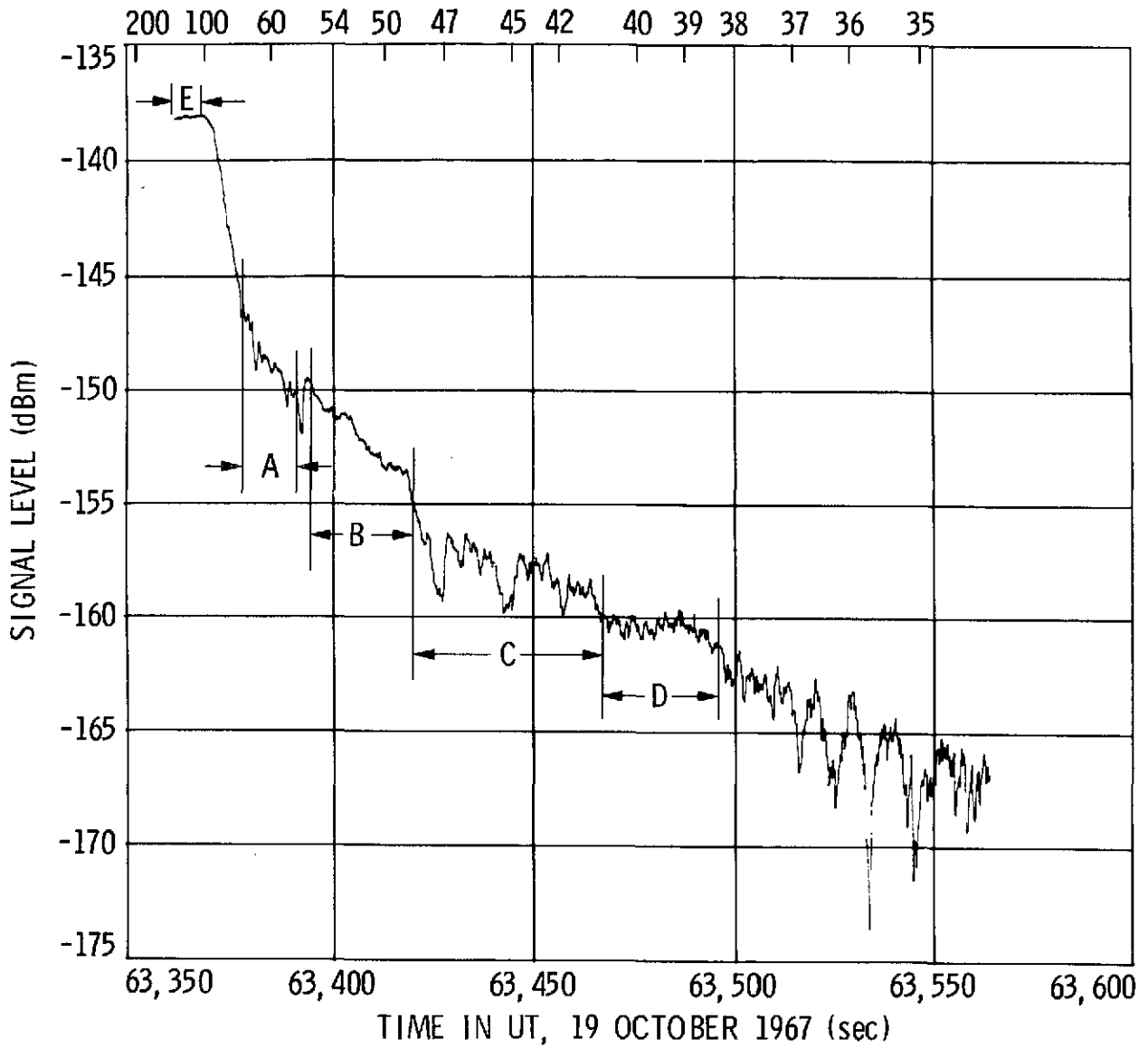Fig. 5. Spectral response of PLL to phase modulation at frequency f

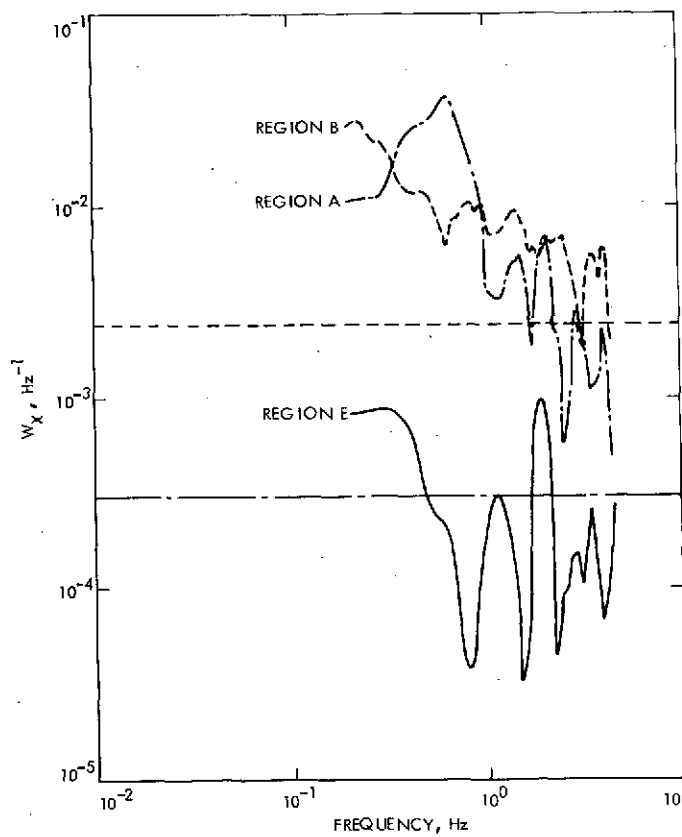Fig. 6. Time history of the signal level for Mariner 5 entrance occultation (from Ref. 7)

Fig. 7. Frequency spectra of the
Mariner 5 log-amplitude fluctua-
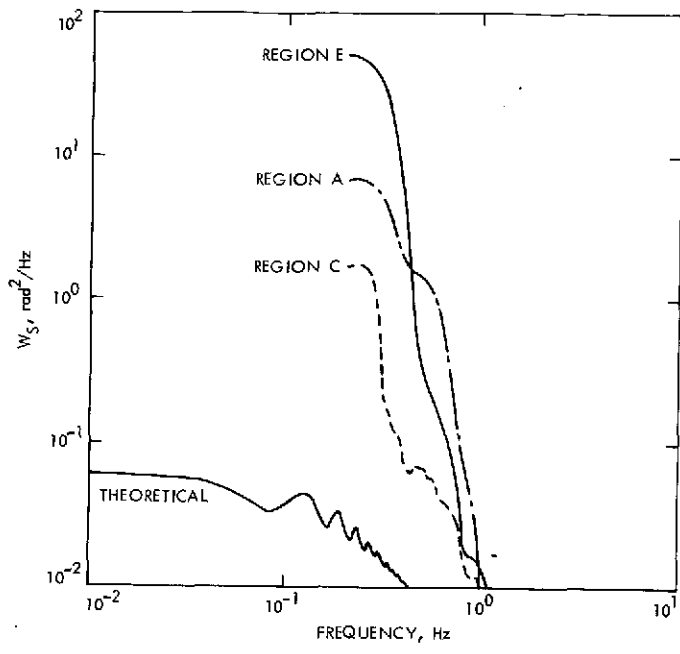tions for regions A, C and E of
entrance occultation

Fig. 8. Frequency spectra of the
Mariner 5 phase fluctuations for
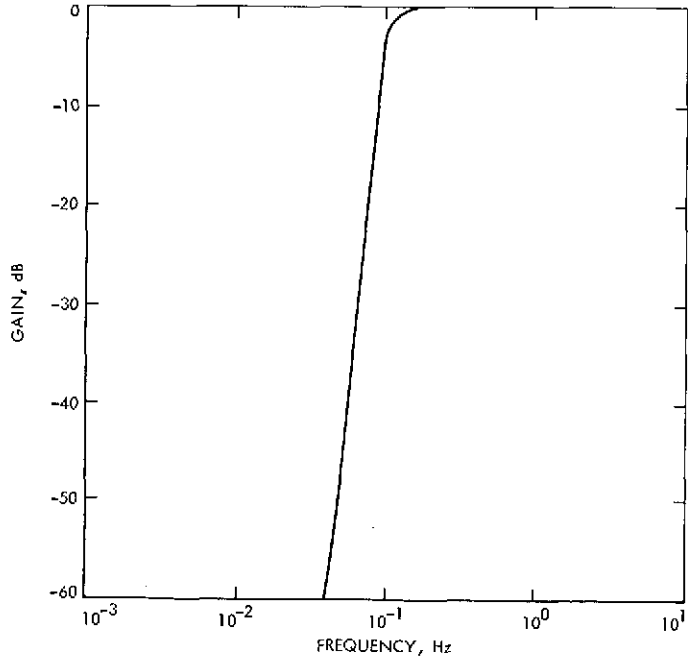regions A, C and E of entrance
occultation

Fig. 9. Frequency response of
eighth-order Butterworth high pass
filter.